atoms

MDPI

Article

Status of CHIP-TRAP: The Central Michigan University High-Precision Penning Trap

Matthew Redshaw [1,2,*], Ramesh Bhandari [1], Nadeesha Gamage [1], Mehedi Hasan [1], Madhawa Horana Gamage [1], Dakota K. Keblbeck [1], Savannah Limarenko [1] and Dilanka Perera [1]

[1] Department of Physics, Central Michigan University, Mount Pleasant, MI 48879, USA; limar1sj@cmich.edu (S.L.)
[2] Facility for Rare Isotope Beams, Michigan State University, East Lansing, MI 48824, USA
* Correspondence: redsh1m@cmich.edu

Abstract: Precise and accurate atomic mass data provide crucial information for applications in a wide range of fields in physics and beyond, including astrophysics, nuclear structure, particle and neutrino physics, fundamental symmetries, chemistry, and metrology. The most precise atomic mass measurements are performed on charged particles confined in a Penning trap. Here, we describe the development, status, and outlook of CHIP-TRAP: the Central Michigan University high-precision Penning trap. CHIP-TRAP aims to perform ultra-high precision (∼1 part in 10^{11} fractional precision) mass measurements on stable and long-lived isotopes produced with external ion sources and transported to the Penning traps. Along the way, ions of a particular m/q are selected with a multi-reflection time-of-flight mass separator (MR-TOF-MS), with further filtering performed in a cylindrical capture trap before the ions are transported to a pair of hyperbolic measurement traps. In this paper, we report on the design and status of CHIP-TRAP and present results from the commissioning of the ion sources, MR-TOF-MS, and capture trap. We also provide an outlook on the continued development and commissioning of CHIP-TRAP.

Keywords: Penning trap; atomic mass; ion source; mass spectrometry

Citation: Redshaw, M.; Bhandari, R.; Gamage, N.; Hasan, M.; Gamage, M.H.; Keblbeck, D.K.; Limarenko, S.; Perera, D. Status of CHIP-TRAP: The Central Michigan University High-Precision Penning Trap. *Atoms* **2023**, *11*, 127. https://doi.org/10.3390/atoms11100127

Academic Editor: Elmar Träbert

Received: 18 August 2023
Revised: 15 September 2023
Accepted: 18 September 2023
Published: 7 October 2023

1. Introduction

1.1. Background and Motivation for CHIP-TRAP

The mass of an atom is one of its fundamental quantities. It directly influences the dynamics of the atomic system under the influence of gravitational and electromagnetic forces but also reflects the effect of nuclear and atomic interactions inside the system through the mass–energy equivalence. As such, atomic masses are required and utilized in a wide range of applications and fields, including metrology, tests of fundamental physics, analytical chemistry, nuclear structure studies, tests of fundamental symmetries, nuclear astrophysics, and in particle and neutrino physics. The necessary degrees of precision to which the atomic masses are required vary from $\sim 10^{-6}$ fractional precision for molecular identification in analytical chemistry, to $\leq 10^{-11}$ for applications to fundamental physics and neutrinos. Over the last three or four decades, the Penning trap has proven to be the most precise and accurate tool for performing atomic mass measurements on a range of nuclides, covering the nuclear chart from the proton to superheavy elements, see, for example [1,2].

The Central Michigan University (CMU) high-precision Penning trap (CHIP-TRAP) is being developed at CMU with the goal of performing ultra-high precision mass measurements ($\leq 10^{-11}$) with applications to neutrinos and tests of fundamental physics. For example, a measurement of the ^{163}Ho electron capture (*EC*) decay *Q* value to a precision of ≈1 eV is important for experiments that aim to determine the electron neutrino mass via electron capture decay spectroscopy with ^{163}Ho [3,4]. In the case of β^- and *EC* decay, the *Q* value

can be directly obtained from the energy equivalent of the mass difference between parent and daughter atoms:

$$Q_{\beta^-/EC} = (M_{\mathrm{P}} - M_{\mathrm{D}})c^2, \tag{1}$$

where M_P and M_D are the masses of the parent and daughter atoms, respectively, and it is understood that the parent and daughter nuclides are not the same for both β^- and *EC* decay (although these decays can have a common parent or daughter). The mass difference can be determined from the mass ratio of ions of the parent and daughter nuclides $R = M_P/M_D$, which is directly measured via Penning trap mass spectrometry (PTMS).

Another example is a direct test of $E = mc^2$. This test can be performed by comparing a Penning trap measurement of the ^{36}Cl–^{35}Cl mass difference with the ^{36}Cl *n*-separation energy obtained from high-precision spectroscopy measurements of γ rays emitted after cold neutron capture on ^{35}Cl [5]. The γ-ray spectroscopy measurement has been performed to a precision of 1.8 eV [6], corresponding to uncertainties of $\approx 4 \times 10^{-11}$ in the masses of ^{35,36}Cl.

1.2. Penning Trap Mass Spectrometry and CHIP-TRAP

An ideal Penning trap consists of a uniform magnetic field and a quadratic electrostatic potential. These fields respectively provide radial and axial confinement for charged particles[1]. Without the presence of the electric field, the radial cyclotron motion of an ion with a charge-to-mass ratio q/m in a magnetic field of strength, B, occurs at the cyclotron frequency:

$$f_c = \frac{qB}{2\pi m}. \tag{2}$$

Hence, the goal of Penning trap mass spectrometry (PTMS) is to determine the mass of an ion via a measurement of f_c. However, the electric field has the effect of reducing the frequency of the cyclotron motion, resulting in the so-called reduced or trap cyclotron motion, with frequency f_+. An additional magnetron radial mode, with frequency f_-, is also introduced due to the $\bar{E} \times \bar{B}$ drift experienced by an ion in the Penning trap. Hence, along with the axial motion with frequency f_z, an ion in the trap undergoes three normal modes of motion. Nevertheless, by measuring and combining the normal mode frequencies, the true cyclotron frequency, f_c of Equation (2), can be reconstructed. The two primary means for doing so are via the Brown–Gabrielse invariance theorem [7],

$$f_c^2 = f_+^2 + f_-^2 + f_z^2 \tag{3}$$

and via the relationship [8]

$$f_c = f_+ + f_-. \tag{4}$$

There are two main categories of techniques used to measure the normal mode frequencies: destructive and non-destructive. The destructive techniques involve probing the ion's motion inside the Penning trap before ejecting it from the trap and detecting it on a sensitive ion detector, typically a microchannel plate (MCP) detector. Destructive measurement techniques include the traditional [9,10] and Ramsey [11–13] variants of the time-of-flight ion cyclotron resonance technique (TOF-ICR), and the more recently introduced phase imaging ion cyclotron resonance (PI-ICR) technique [14,15]. Compared to non-destructive techniques, destructive techniques are typically more compatible with mass measurements on short-lived isotopes produced at accelerator facilities and transported to the Penning trap (on-line Penning trap facilities) [1,2]. Non-destructive techniques involve detecting the ion inside the Penning trap via the image currents it induces in the trap electrodes used to create the quadratic electrostatic potential. These techniques have been used mainly for ultra-high precision measurements with stable isotopes, with ions being produced inside the Penning trap by ionizing gases or vapors admitted to the trap (off-line Penning trap facilities); see [16–19].

CHIP-TRAP aims for ultra-high precision measurements with stable and long-lived isotopes. Ions are produced in external ion sources and transported to the Penning trap. This will provide access to a wide range of isotopes and enable the use of techniques developed at on-line Penning trap facilities to efficiently select a minority population of ions of interest. This will enable measurements with isotopes that are only available in small quantities. The CHIP-TRAP measurement trap will consist of a pair of hyperbolic traps that will employ simultaneous measurements using a phase-sensitive image charge detection technique. This will reduce statistical uncertainty due to temporal magnetic field fluctuations.

2. Materials and Methods

A CAD drawing of the CHIP-TRAP apparatus is shown in Figure 1. The CHIP-TRAP apparatus consists of two ion sources, a transport beamline that includes a multi-reflection time-of-flight mass separator (MR-TOF-MS), microchannel plate (MCP) detectors, a 12 T superconducting magnet that houses the CHIP-TRAP Penning traps, and a pulse tube cold head for cooling the Penning traps to 4 K.

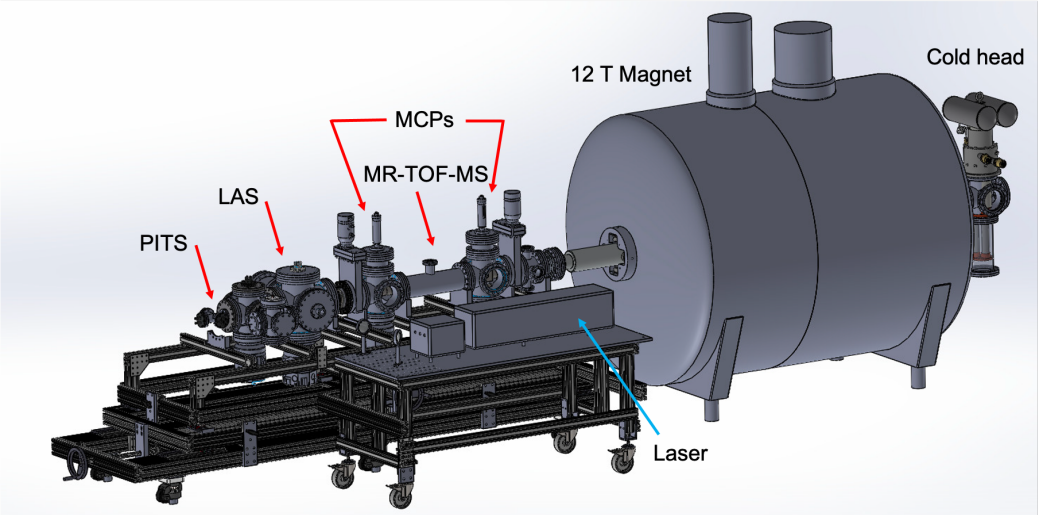

Figure 1. CAD drawing of the CHIP-TRAP apparatus. The main components include a Penning ion trap source (PITS), a laser ablation source (LAS), microchannel plate (MCP) detectors for ion beam detection, a multi-reflection time-of-flight mass separator (MR-TOF-MS) for separating ions of different nominal m/q, a 12 T superconducting magnet that houses the Penning traps, and a cold head for cooling the traps down to 4 K.

The two ion sources that CHIP-TRAP employs are a laser ablation ion source (LAS) for producing ions from solid target materials, and a Penning ion trap source (PITS) that uses electron impact ionization to produce ions from gaseous materials. These are described in more detail below. After ions are extracted from one of the ion sources, they are directed into the main beam line and enter the MR-TOF-MS, which can be used to resolve ions of a particular nominal m/q. Next, the ions enter the bore tube of a 12 T superconducting solenoidal magnet and are first captured in a cylindrical capture/filter trap for ion identification and the removal of isobaric contaminant ions. The remaining ions of interest are then transported to a pair of hyperbolic geometry measurement traps for precision mass measurements.

2.1. Ion Sources

2.1.1. Laser Ablation Source (LAS)

Since it was first used in conjunction with a Penning trap at the ISOLTRAP facility around 2002 [20], the LAS has become a staple for ion production for many on-line Penning traps [21–25]. The LAS can be used to conveniently provide ions from essentially any

solid source material or from a solution dried out on a metal backing plate, e.g., [26–29]. Measurements at Penning trap facilities with ions from a LAS have spanned the nuclear chart from, for example, ^{6,7}Li [30] to ^{249}Cf [28]. Ions from a LAS serve as reference masses for on-line measurements with short-lived isotopes, calibrants for tuning a system and investigating systematics, and as the ions of interest for nuclear and neutrino physics studies, e.g., [31–37].

A LAS requires a high-powered pulsed laser that is focused to a small spot size (typically $\leq$1 mm diameter), which provides a power density of $\sim 10^8$ W/cm^2 to enable ablation. For a standard nanosecond pulse length laser, this corresponds to an energy density of $\sim$0.1–1 J/cm^2. The high energy density laser pulse causes the evaporation of material from the surface of the target followed by ionization due to the high temperatures that are generated. The CHIP-TRAP LAS uses a Continuum Surelite II frequency-doubled 532 nm pulsed Nd:YAG laser [38], which has a 5 ns pulse duration and energy output of up to 160 mJ at 532 nm. A schematic and picture of the CHIP-TRAP LAS are shown in Figure 2.

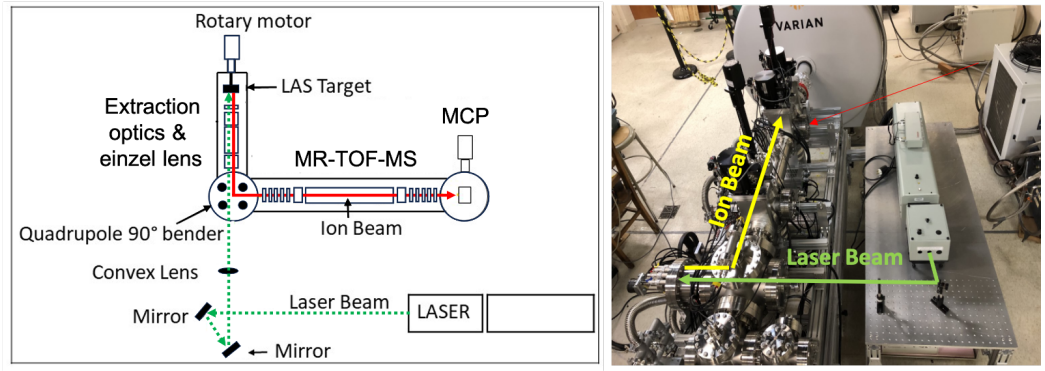

Figure 2. Left: Schematic drawing of the LAS indicating the path of the laser beam (green dashed line) and ion beam (red solid line). **Right**: photo of the CHIP-TRAP beamline, showing the laser used for the LAS, vacuum chamber housing for the LAS, 8″ 6-way cross that houses the quadrupole bender, and beamline housing the MR-TOF-MS, followed by the injection beamline to the 12 T magnet.

After ions are produced at the surface of the target, they are extracted by accelerating them to 4 keV via an extraction cylinder and plate. They are then transported at 1 keV through an einzel lens and focused into an electrostatic quadrupole bender that bends them 90° into the main beamline. The design of the extraction optics is based on Ref. [24], and further details can be found in Refs. [39,40]. The CHIP-TRAP LAS was commissioned and used to generate $^{12}C_n^+$ clusters from a Sigradur® [41] glassy carbon target [40], singly charged ions of metals from ^{7}Li$^+$ to ^{197}Au$^+$, and Mg$^+$, Ca$^+$, and ^{165}Ho$^+$ ions from solutions that were dried out on a backing target [29].

2.1.2. Penning Ion Trap Source (PITS)

At Central Michigan University, we developed a so-called Penning ion trap source (PITS) that produces ions via the electron impact ionization of gaseous samples [40,42]. The ionization occurs inside a cylindrical Penning trap. Hence, the ions are automatically confined in a small volume after production and can be released as a pulsed beam. A cross-sectional view of the PITS is shown in Figure 3 (left).

The PIT source Penning trap consists of a cylindrical ring electrode and two circular endcaps and is housed inside the 1.27 cm diameter bore of a 4.45 cm diameter $\times$ 1.27 cm thick 0.55 T NdBFe ring magnet [43]. As such, it is an uncompensated Penning trap. However, the ratio of the trap radius to height, ρ_0/z_0 = 1.20, with ρ_0 = 5.35 mm and z_0 = 4.45 mm, was chosen to minimize the lowest-order electrostatic field imperfection, characterized by the C_4 parameter [44]. The end caps have 2 mm diameter holes in them to allow the electron beam to enter from the injection side and to allow ions to be extracted from the ejection side. The electron beam is produced by thermal emission from a tungsten

filament [45] that is biased at ≈10–30 V to define the energy of the electron beam. Further details on the CHIP-TRAP PITS can be found in Refs. [40,42,46].

During ion production, a potential of 5 V is applied to the end cap electrodes, while the ring electrode is held at the ground. To release the ions, the end cap on the ejection side of the PIT is set to 0 V, while the injection side is held at 5 V. A series of extraction electrodes helps to extract ions from the trap region and accelerates them to an energy of ≈1 keV. Next, ions are focused into an electrostatic quadrupole bender by an einzel lens and are steered into the main beamline. The PIT source was commissioned and used to create and extract ions produced from the residual background gas in the vacuum, and from noble gases, helium, neon and argon, that were admitted to the PIT source [46].

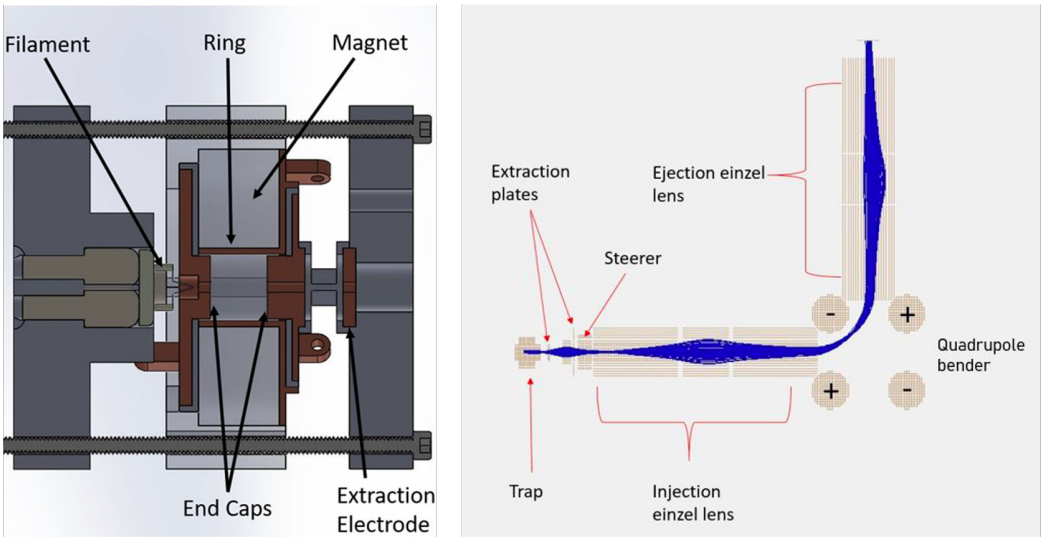

Figure 3. Left: Cross-sectional CAD drawing of the PITS. The filament that produces the electron beam is located next to the end cap on the left. The ring electrode is housed inside the bore of the NdBFe magnet and ions that are produced inside the PITS are extracted through the end cap on the right. **Right**: Simulated path of ions after they are produced in the PITS, then extracted, focused into a quadrupole bender, and steered into the main beamline.

2.2. Multi-Reflection Time-of-Flight Mass Separator (MR-TOF-MS)

If a pulsed beam consisting of ions with a range of m/q ratios is accelerated to an initial (non-relativistic) energy $E = qV$ through a potential V, and allowed to propagate over a distance L, then the different m/q ions will separate according to their time of flight (TOF):

$$t_{TOF} = \frac{L}{\sqrt{2V}}\sqrt{\frac{m}{q}}. \tag{5}$$

Hence, ions of different m/q can be temporally resolved in this way. However, there are two main issues with this procedure. Firstly, providing a long path length L can be expensive and takes up valuable lab space, and secondly, the temporal spread Δt of the ion bunch also increases with distance. The multi-reflection time-of-flight mass separator (MR-TOF-MS) addresses both of these problems by operating as an ion trap, folding the ion path on top of itself via a pair of electrostatic mirrors, and by re-focusing the ion bunch on each turn in the MR-TOF-MS to minimize increases in Δt. Over the last decade or so, MR-TOF-MSs have been introduced in on-line accelerator facilities as mass separators to prepare ion beams before mass measurements with Penning traps [47] and as mass spectrometers themselves, e.g., [48].

The CHIP-TRAP MR-TOF-MS design is based on the Notre Dame MR-TOF-MS [49] but with an overall length of 49 cm vs. 79 cm due to the size constraints in the CHIP-TRAP beamline. A schematic and picture of the CHIP-TRAP MR-TOF-MS are shown in Figure 4.

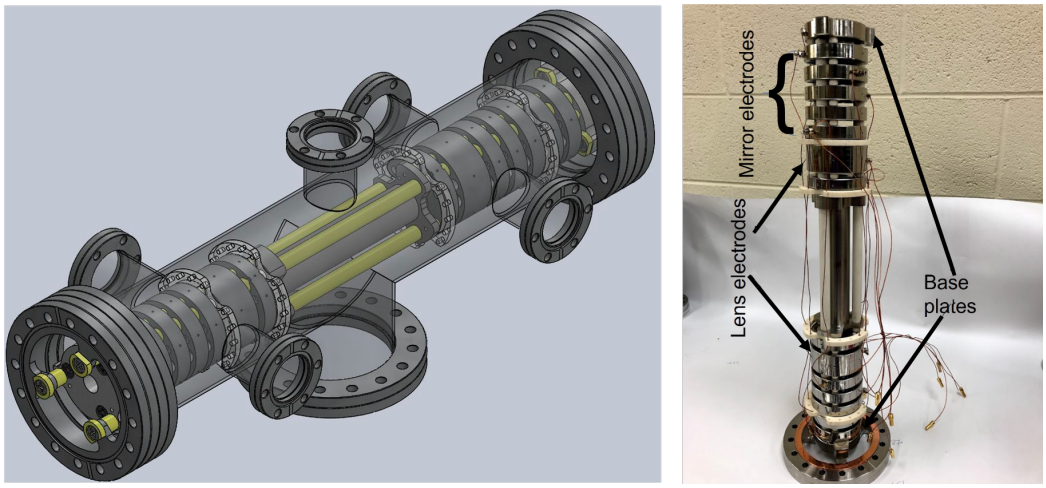

Figure 4. Left: CAD drawing of the MOR-TOF-MS. Support rods and insulators are in green and electrodes are in grey. The MR-TOF-MS electrodes are housed inside a 6″ vacuum tube. **Right**: picture of assembled electrode structure attached to a 6″ conflat flange.

The device consists of one central drift tube, a pair of lens electrodes, five pairs of mirror electrodes, and a pair of base plates. In trapping mode, the central drift tube is held close to the ground potential. The lens and the mirror closest to it are at negative potentials, and the next four mirror electrodes are at progressively more positive potentials as shown in Figure 5.

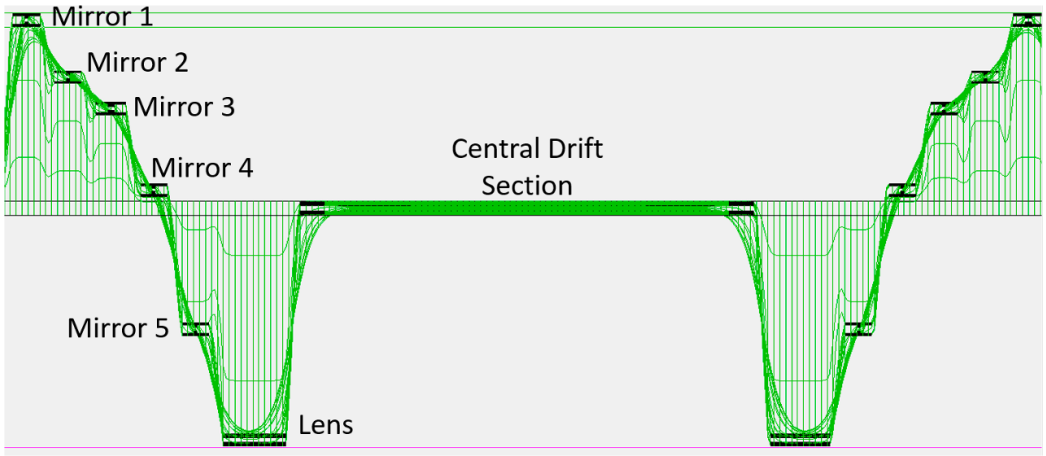

Figure 5. Cross-section of equipotentials in the CHIP-TRAP MR-TOF-MS. The central drift tube section is held at ground potential druing trapping but is raised to 2.8 kV in order to trap and release ions from the MR-TOF-MS. The lens is at −2.3 kV, and mirror 1 at +2.9 kV.

In order to admit and trap ions, the "in-trap potential lift" scheme is used [50]. The ion beam is transported toward the MR-TOF-MS with an energy of ≈1 keV. A cylindrical lift electrode located before the entrance to the MR-TOF-MS is quickly switched from −1 kV to 3 kV when the ion bunch enters it. At this time, the central drift tube is raised from ground to 2.8 kV. Hence, the ions then enter the MR-TOF-MS with enough energy to pass the +3 kV mirror electrode at the entrance to the MR-TOF-MS. When the ions reach the center of the central drift tube, its potential is lowered to ground, reducing the energy of the ions so that they then become trapped in the MR-TOF-MS potential. The ions are confined for a certain number of cycles as required by the user and then released by again raising the potential of the central drift tube to 2.8 kV when the ions are at the center of the tube, and traveling toward the ejection end of the MR-TOF-MS. The ions can then pass over the ejection Mirror 1 electrode. After they exit the MR-TOF-MS, they enter another cylindrical lift electrode that is held at 3 kV and lowered to −1 kV to reduce the ion beam's energy back to the 1 keV

transport energy. The ions are then focused onto an MCP for TOF analysis. We plan to use a Bradbury–Nielsen gate (BNG) [51] to allow the ions of a particular m/q to pass and be injected into the magnet bore toward the Penning traps, and to remove unwanted ions from the beam.

2.3. CHIP-TRAP Penning Traps

The CHIP-TRAP Penning trap system is comprised of three Penning traps: a cylindrical geometry capture/filter trap, and two hyperbolic geometry measurement traps. A picture of the assembled trap structure before the electrodes were gold-plated is shown in Figure 6 (left).

An ion bunch from one of the ion sources (after m/q analysis and selection with the MR-TOF-MS) will be transported into the magnet bore, and captured in the capture trap. This trap will be used to identify ions that have been captured using Fourier transform ion cyclotron resonance (FT-ICR) techniques [52–54]. It will then be used to remove any unwanted ions before transporting the ions of interest to one of the measurement traps. After a pair of ions of different species has been loaded into the two measurement traps, a cyclotron frequency ratio measurement will be performed.

Figure 6. Pictures of the CHIP-TRAP Penning traps. **Left**: the assembled hyperbolic measurement traps stacked on top of the capture trap before the electrodes were gold plated. **Middle**: the cylindrical capture trap after gold plating, consisting of two end caps, two correction ring electrodes and quartered ring electrodes. **Right**: the hyperbolic measurement traps after gold plating, consisting of hyperbolic ring and end-cap electrodes, quartered correction ring electrode and correction tube electrodes. The two traps are stacked together in the bottom picture. Sapphire insulating rings can also be seen in the pictures.

2.3.1. Capture Trap

The capture trap is an orthogonally compensated, cylindrical geometry Penning trap with a closed end-cap design. A picture of the capture trap after gold plating is shown in Figure 6 (middle). The top picture shows the two end caps, two correction rings, and quartered ring electrode, and the bottom picture shows the assembled trap. A schematic of the trap is also shown in Figure 7. The trap has an axial length of $2z_0 = 25.2$ mm and radius of $\rho_0 = 15.0$ mm, resulting in a characteristic trap size,

$$d = \sqrt{\rho_0^2/4 + z_0^2/2}, \tag{6}$$

of 11.65 mm. The end caps each have $d_0 = 3$ mm diameter holes in their centers to facilitate ion injection and ejection. The quartered ring electrode enables an RF dipole drive to be applied across two of the opposing ring segments, while the remaining two ring electrodes are used for ion detection.

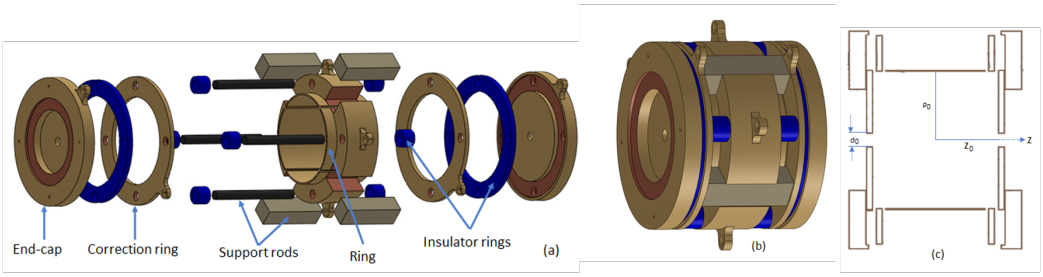

Figure 7. Schematic drawing of the capture trap: (**a**) exploded view—copper-colored components are the electrodes, blue components are insulators, and brown components are insulated support rods; (**b**) assembled view; (**c**) cross-sectional outline with labeled dimensions.

After a bunch of ions are captured in the capture/filter trap, they are first identified via their m/q ratio using the FT-ICR technique. This is performed by applying a broadband RF dipole frequency sweep excitation to drive the mass-dependent, reduced cyclotron motion of the ions. Broadband detection of the image currents induced in the trap electrodes is then performed. For this, we employ a Stahl FTICR-3 low-noise pre-amplifier [55]. The analogue voltage signal from the amplifier is digitized with a National Instruments oscilloscope card (PXI-5114), and fast Fourier transform (FFT) is performed in LabView software. The resulting peak signals in the frequency domain correspond to the reduced cyclotron frequencies of the ions that are present in the trap. By first calibrating the magnetic field by determining the frequency of an ion or ions of known m/q, the corresponding m/q of ions for all observed peaks can be determined. In subsequent capture cycles, previously identified and unwanted ions that are present in the capture trap can be removed by applying an RF dipole cleaning scheme: either by targeting the f_+ of the previously observed contaminant ions, or by applying the broadband SWIFT cleaning scheme [56–58] around the reduced cyclotron frequency of the ion of interest. By lowering the voltage on the end cap of the capture trap and of the measurement trap, ions can be released from the capture trap and will then enter the measurement trap, where they can be recaptured.

2.3.2. Measurement Traps

The measurement traps are orthogonally compensated hyperbolic geometry Penning traps that also include a correction tube electrode. A picture of the measurement traps after gold plating is shown in Figure 6 (right). The bottom picture shows the assembled stacked traps, and the top picture shows, for one of the traps, the two correction tubes, two end caps, ring electrode, and the two four-way segmented correction ring electrodes. A schematic of the measurement trap is shown in Figure 8. It is based on the design of the single-ion Penning trap (SIPT) [59], which is part of the low energy beam and ion trap (LEBIT) Penning trap apparatus [60] at the Facility for Rare Isotope Beams (FRIB). The measurement traps have an axial length $2z_0$ = 11.2 mm and radius ρ_0 = 6.5 mm, resulting in a characteristic trap size d = 5.11 mm. The end caps have $d_0 = 1$ mm diameter holes to enable ion injection and ejection to transport ions between the traps.

The proposed measurement scheme is to perform simultaneous frequency measurements on pairs of ions in the two precision measurement traps. The frequency measurements are made using the pulse and phase (PNP) technique originally developed at MIT [17,61]. This method is an extension of the two-ion technique developed at MIT, in which simultaneous PNP cyclotron frequency measurements are made on pairs of ions confined on a common magnetron orbit in a single Penning trap [62–64]. Like the MIT simultaneous two-ion technique, the proposed CHIP-TRAP two-ion technique will greatly reduce the effect of magnetic field fluctuations that typically limit the achievable statistical precision when performing alternating measurements on the two species. However, unlike in the MIT two ion technique, ions in the CHIP-TRAP Penning traps will be located at the center of the traps. This will greatly reduce the contribution of systematic shifts and uncertainties in the measurement due to the effect of magnetic and electric field imperfections

combined with the relatively large (≈1 mm diameter) magnetron amplitude necessary for the MIT two-ion technique. An obvious new source of systematic error in this technique is due to the fact that the two ions, now in separate traps, will not experience the same electric and magnetic field. This limitation can be mitigated by performing a series of measurements in which the ions are switched between the two traps.

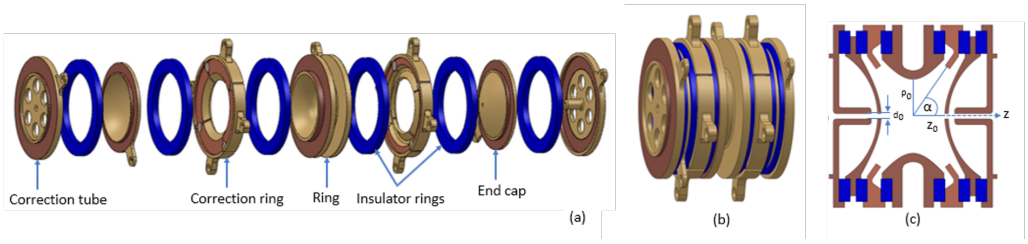

Figure 8. Schematic drawing of a measurement trap: (**a**) exploded view—copper colored components are the electrodes, blue components are insulators, and brown components are insulated support rods; (**b**) assembled view; (**c**) cross-sectional outline with labeled dimensions.

3. Results

3.1. LAS

The LAS was initially commissioned in a test stand [40] and then installed in the CHIP-TRAP beam line; see Figure 2. Initial commissioning in both cases was performed by using carbon cluster ions as described in Section 2.1.1. The ions were transported along the beam line, and their arrival time at the MCP detector was recorded. This enabled a TOF spectrum to be built up from repeated cycles of ion production from the pulsed laser. An example TOF spectrum for $^{12}C_n^+$ ions is shown in Figure 9 (left). Equation (5) was used to estimate the TOF for the $^{12}C_n^+$ ions and make an initial identification of the peaks in Figure 9 (left). This identification, and the confirmation of Equation (5) was made by plotting TOF vs. $(m/q)^{1/2}$ as shown in Figure 9 (right). The location of the $^{12}C_n^+$ peaks clearly follows the expected relationship. Interestingly, the TOF of the first peak was consistent with an m/q = 13 u/e rather than 12 u/e for $^{12}C^+$ ions. Hence, we assume this peak to be due to $^{12}CH^+$.

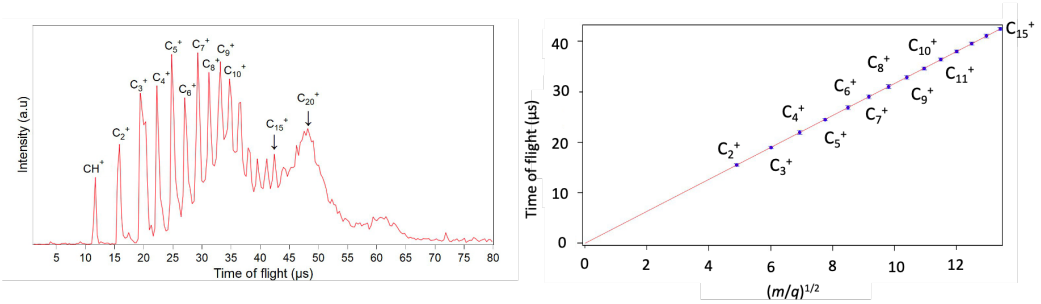

Figure 9. Left: time-of-flight (TOF) spectrum for carbon cluster ions produced with the LAS and recorded on the MCP detector. **Right**: TOFs obtained from fits to the peaks in the TOF spectrum plotted vs. $(m/q)^{1/2}$ of the inferred $^{12}C_n^+$ ions.

After this initial commissioning, we tested ion production from metal targets, which were typically 2.5 cm × 2.5 cm × ≈ 1 mm thick. We investigated production from a range of materials, including Al, Fe, Ni, Zn, Ag, In, Ho, W and Au. An example of a TOF spectrum for Zn ions is shown in Figure 10 (left). As can be seen for Zn, atomic ions were the dominantly produced ions, but dimer ions were also observed. For lighter ions, such as Zn^+, peaks corresponding to the different isotopes were observed. For heavier ions, such as Ag^+, W^+, and Au^+, the different isotopes could not be resolved, and a single, broad peak was observed in the TOF spectrum. As with the $^{12}C_n^+$ clusters, we produced a plot of TOF vs. $(m/q)^{1/2}$, which is shown in Figure 10 (right) for the metal target ions. Again, TOF vs. $(m/q)^{1/2}$ followed the expected linear relationship of Equation (5).

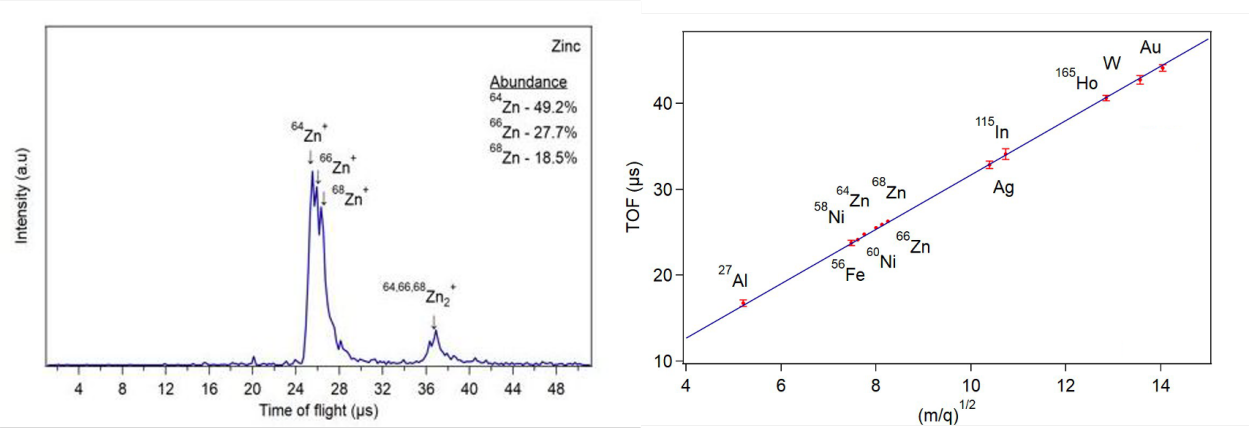

Figure 10. Left: time-of-flight (TOF) spectrum for zinc ions produced with the LAS and recorded on the MCP detector. **Right**: TOFs obtained from fits to the peaks in the TOF spectra obtained for the different metal target ions plotted vs. $(m/q)^{1/2}$. When TOF peaks for the different isotopes of an element could not be resolved, a weighted average m/q based on natural abundances was used.

Finally, we also tested the production of $^{165}Ho^+$ ions using solutions of holmium nitrate ($Ho[NO_3]_3$). These solutions were made by dissolving holmium metal powder in 6 M nitric acid. We investigated the use of different backing metals on which to dry the $Ho[NO_3]_3$ solution to determine the relative amounts of $^{165}Ho^+$, $^{165}HoO^+$, $^{165}HoO_2^+$, and the backing material ions that were produced. We also studied the minimum quantity of Ho atoms required in the sample to produce ions. We found that a nickel backing target was optimal in terms of maximizing the fraction of $^{165}Ho^+$ ions produced, minimizing the amount of (Ni^+) background ions produced, and minimizing the amount of ^{163}Ho material required [29].

3.2. PITS

Initial commissioning of the PITS involved producing ions inside the trap region by ionizing residual gas in the vacuum (measured to be $\approx 10^{-8}$ mbar with a nearby Penning gauge). The ions were successfully ejected from the trap, steered through the beamline and detected on the second MCP shown in Figure 1. The ion bunch observed on the MCP had a width of 2.5 µs (see Figure 11) and a TOF of ≈32 µs. We also observed a smaller peak at ≈8 µs with a width of 0.6 µs, also shown in Figure 11.

Next, we made ions by leaking noble gases He, Ar, and Ne into the trapping region. This raised the pressure as read by the nearby Penning gauge to $\approx 10^{-6} - 10^{-7}$ mbar. We were able to identify peaks due to He^+ and Ar^+ ions, but the Ne^+ peak overlapped with that of the residual gas ion peak and could not be resolved. A second peak also appeared with a TOF of ≈40 µs when leaking gas samples into the trap; see Figure 11. Using $^4He^+$ and $^{40}Ar^+$ to calibrate the TOF spectrum, the peak at 8 µs was determined to be $^1H^+$. Data for these three ions were then used to make a calibration curve, from which we determined the residual gas ion peak to correspond to m/q = 17.9(6) u/e and the leaked gas ion peak to m/q = 28.0(1.0) u/e. Hence, the residual gas ions are likely H_2O^+ or perhaps H_3O^+, and the leaked gas ions N_2^+. These findings are consistent with the typical residual gas makeup in a vacuum system that has not been baked [65,66], and with air being leaked into the vacuum system along with the noble gases. Further details of the commissioning of the PITS can be found in Ref. [46] and will appear in a forthcoming publication.

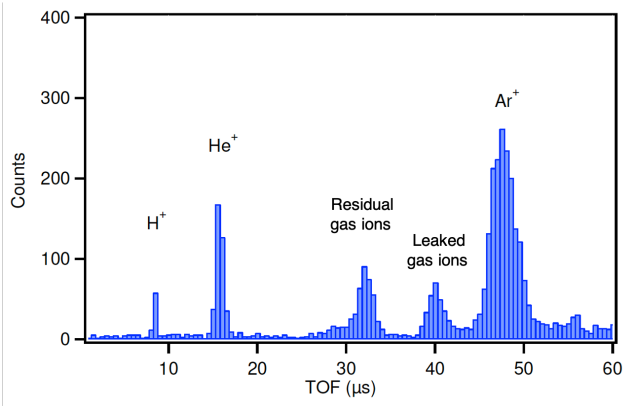

Figure 11. Time-of-flight spectrum for ions produced with the PITS and detected on the MCP. The residual gas ions were identified as H_2O^+ or H_3O^+, and the leaked gas ions as $^{14}N_2^+$

3.3. MR-TOF-MS

Initial commissioning of the MR-TOF-MS was performed using ions produced with the LAS. We were able to successfully implement the "in-trap lift" method [50] to capture and release ion bunches in the MR-TOF-MS. We manually tuned the timing and voltage settings for the MR-TOF-MS to maximize efficiency and resolving power, i.e., reduce losses over as long of a capture time as possible. Our initial investigations focused on trapping $^{27}Al^+$ ions. We were able to trap $^{27}Al^+$ for 1000 cycles in the MR-TOF-MS, corresponding to a trapping time of ≈9 ms and a path length ∼500 m. We observed a linear increase in resolving power $R = t_{TOF}/2\Delta t$ vs. cycle number, reaching $R \approx 2500$ after 1000 cycles, as shown in Figure 12 (left). However, as can be seen in Figure 12 (right), the count rate quickly drops off within the first 200 cycles. This is due to the fact that the initial spread of the pulsed beam from the LAS is larger than the acceptable spread for trapping in the MR-TOF-MS.

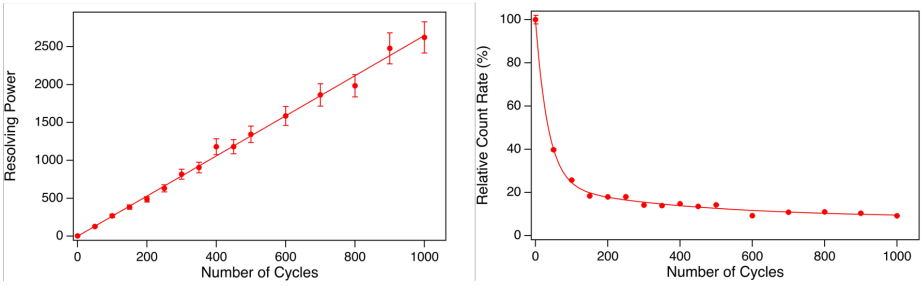

Figure 12. Left: Resolving power vs. number of cycles stored in the MR-TOF-MS for $^{27}Al^+$ ions. The solid line is a linear fit to the data. **Right**: Count rate of $^{27}Al^+$ ions detected on the MCP vs. number of cycles relative to the count rate when the ions were stored for zero cycles. The solid line is a double exponential fit to guide the eye.

3.4. Capture Trap

We located the capture trap in the center of the 12 T magnet and installed a LaB_6 thermionic electron emitter [67] behind the ejection side of the capture trap. When heated, the LaB_6 cathode emits an electron beam that travels through the capture trap, ionizing residual gas in the capture trap and creating ions that are automatically confined. To identify ions, we first used an rf dipole drive close to the mass-independent magnetron frequency f_- to excite the magnetron motion of trapped ions, driving them to a magnetron orbit of radius ρ_-. These ions could then be detected via the image currents they induced in the trap electrodes using a differential amplifier. We initially used an NF Corp SA-421F5 Low Noise FET Differential Amplifier [68] and later the Stahl FTICR3 preamplifier [55].

After confirming that we could create and detect ions, we looked for the mass-dependent reduced-cyclotron motion by using a dipole drive sweep near the cyclotron

frequency f_+ of H_3O^+. This ion species was chosen since it was expected to be present when ionizing residual background gas as observed previously in other systems, e.g., [65,66]. We did observe a peak at $f_+ \approx 9.69$ MHz, consistent with that of an ion having $m/q = 19$ in an ≈12 T magnetic field. In addition to the peak at 9.69 MHz in the frequency spectrum, we also observed sidebands at about 1.8 kHz higher and lower in frequency than the f_+ peak; see Figure 13. These sidebands are a result of the ions also having magnetron motion with frequency f_-, resulting in frequency components at $(f_+ \pm f_-)$ in the FFT [69]. The presence of magnetron motion when it is not explicitly driven is likely due to ions not being made at the trap center or from self-excitation of the ion cloud. Additional studies with the capture trap included the characterization of the capture trap trapping potential by measuring f_+ and f_- as a function of ρ_+ and ρ_-, respectively, for different correction electrode voltages. This method can be used to "tune" the trap so as to minimize the lowest-order electrostatic field imperfection, characterized by the C_4 parameter [18,44,62]. Further details are available in Ref. [70] and will be presented in a forthcoming publication.

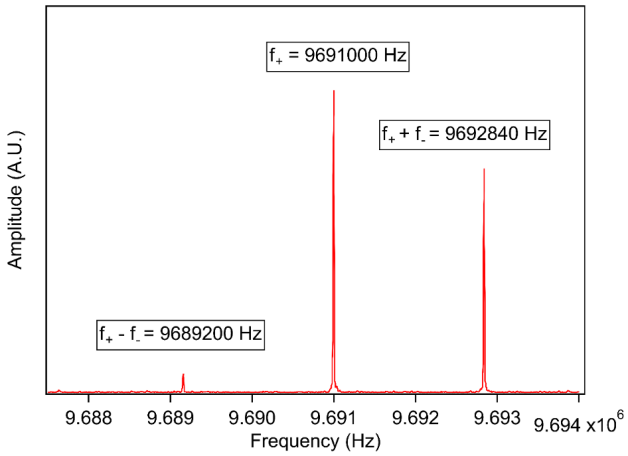

Figure 13. Fast Fourier transform of image charge signal induced after creating H_3O^+ ions and driving them with an rf dipole drive close to their reduced cyclotron frequency, f_+. The central peak corresponds to f_+, while the left and right peaks correspond to sidebands at $f_+ \pm f_-$.

4. Discussion

Over the last several years, we have successfully commissioned a laser ablation ion source (LAS) and a new, novel Penning ion trap (PIT) source. The LAS has proven to be a robust and versatile ion source able to make ions from a wide range of solid metal targets. The LAS has also been used to make ions from the residual material left behind by a metal-containing solution dried out on a backing plate, e.g., Ho^+ ions from a $Ho(NO_3)_3$ solution. These studies indicate feasibility for anticipated measurements with CHIP-TRAP, such as with the long-lived isotope ^{163}Ho for neutrino physics applications. The PIT source has been used to demonstrate the ability to create pulsed ion beams from electron impact ionization of gaseous sources. This provides access to materials that are not available in solid form. Future modifications could also include the ability to produce ions from vaporized sources. The PIT source could be used in future proposed measurements with CHIP-TRAP to measure the ^{36}Cl–^{35}Cl mass difference for a test of $E = mc^2$ by creating ions from HCl gas or a vaporized NaCl sample.

More recently, we designed, fabricated, assembled and commissioned a multi-reflection time-of-flight mass separator (MR-TOF-MS). During initial commissioning, this device was used to trap a bunch of $^{27}Al^+$ ions for 1000 cycles, providing a resolving power of about 2500. Future improvements will involve a more robust tuning scheme with automated data acquisition. This could lead to more optimal voltage settings to increase resolving power and efficiency. It could also be possible to develop and install a gas-filled RF quadrupole trap to cool and bunch the ion beam before sending it to the MR-TOF-MS. This could reduce

the emittance and initial temporal spread of the ion bunch, leading to improved efficiency and resolving power.

We also successfully completed the initial commissioning of the capture/filter trap, which is a compact cylindrical trap design with flat end caps. We produced ions inside the trap via electron impact ionization of residual background gas in the vacuum, and identified these ions as H_3O^+. We tested a low noise differential amplifier, operated at room temperature and located in the fringe field of the 12 T magnetic field. The amplifier will next be tested inside the bore of the magnet, under vacuum, and located at a position where the B-field is 6 T (per the manufacturer's stated operating parameters).

Further goals for the continued development and commissioning of CHIP-TRAP include the installation of ejection optics and an MCP to aid tuning the injection optics to capture ions from the LAS and PITS in the capture trap. We also plan to perform TOF-ICR measurements on ions using the capture trap. Next, we will install and commission a cooling apparatus based on a pulse tube cryocooler to cool the traps and FT-ICR amplifier down to ≈4–5 K. Finally, we will commission the measurement traps and the proposed SQUID detection scheme for the detection of image currents in the measurement trap end-cap electrodes, and we will prepare for the first mass measurements with CHIP-TRAP.

Author Contributions: Conceptualization, M.R.; methodology, N.G., R.B., M.H.G., M.H., D.K.K., D.P. and S.L.; software, N.G., M.H.G. and R.B.; formal analysis, N.G., M.H.G. and R.B.; investigation, N.G., R.B., M.H.G., M.H., D.K.K., D.P. and S.L.; original draft preparation, M.R.; writing—review and editing, M.R., N.G., R.B., M.H.G., M.H., D.K.K., D.P. and S.L.; supervision, M.R.; project administration, M.R.; funding acquisition, M.R. All authors have read and agreed to the published version of the manuscript.

Funding: This material is based upon work supported by the US Department of Energy, Office of Science, Office of Nuclear Physics under Award No. DE-SC0015927 and No. DE-SC0022538, and by the National Science Foundation under Contracts No. PHY-1307233, PHY-1607429, and PHY-2111302, and by Central Michigan University.

Acknowledgments: We thank Ray Clark and Mark Wilson for the technical assistance.

Conflicts of Interest: The authors declare no conflict of interest

Note

[1] Here, we consider only positive ions, although negative ions and other charged particles can be trapped.

References

1. Blaum, K. High-accuracy mass spectrometry with stored ions. *Phys. Rep.* **2006**, *425*, 1–78. [CrossRef]
2. Blaum, K.; Dilling, J.; Nörtershäuser, W. Precision atomic physics techniques for nuclear physics with radioactive beams. *Phys. Scr.* **2013**, *2013*, 014017. [CrossRef]
3. Gastaldo, L. *Et Al.*, E.C. Electron Capture ^{163}Ho Exp.—ECHo. *Eur. Phys. J. Spec. Top.* **2017**, *226*, 1623. [CrossRef]
4. Faverzani, M.; Alpert, B.; Backer, D.; Bennet, D.; Biasotti, M.; Brofferio, C.; Ceriale, V.; Ceruti, G.; Corsini, D.; Day, P.K.; et al. The HOLMES Experiment. *J. Low Temp. Phys.* **2016**, *184*, 922. [CrossRef]
5. Dewey, M.S.; Kessler, E.G.K., Jr.; Deslattes, R.D.; Börner, H.G.; Jentschel, M.; Doll, C.; Mutti, P. Precision measurement of the ^{29}Si, ^{33}S, and ^{36}Cl binding energies. *Phys. Rev. C* **2006**, *73*, 044303. [CrossRef]
6. Krempel, J. A New Spectrometer to Measure the Molar Planck Constant. Ph.D. Thesis, Ludwig-Maximilians-Universität, Munich, Germany, 2010. Available online: https://edoc.ub.uni-muenchen.de/13202/ (accessed on 8 August 2023).
7. Brown, L.S.; Gabrielse, G. Precision spectroscopy of a charged particle in an imperfect Penning trap. *Phys. Rev. A* **1982**, *25*, 2423–2425. [CrossRef]
8. Gabrielse, G. Why Is Sideband Mass Spectrometry Possible with Ions in a Penning Trap? *Phys. Rev. Lett.* **2009**, *102*, 172501. [CrossRef]
9. Gräff, G.; Kalinowsky, H.; Traut, J. A direct determination of the proton electron mass ratio. *Z. Phys. A Atoms Nucl.* **1980**, *297*, 35–39. [CrossRef]
10. König, M.; Bollen, G.; Kluge, H.J.; Otto, T.; Szerypo, J. Quadrupole excitation of stored ion motion at the true cyclotron frequency. *Int. J. Mass Spectrom. Ion Process.* **1995**, *142*, 95–116. [CrossRef]
11. Bollen, G.; Kluge, H.J.; Otto, T.; Savard, G.; Stolzenberg, H. Ramsey technique applied in a Penning trap mass spectrometer. *Nucl. Instrum. Methods Phys. Res. Sect. B Beam Interact. Mater. Atoms.* **1992**, *70*, 490–493. [CrossRef]

12. George, S.; Blaum, K.; Herfurth, F.; Herlert, A.; Kretzschmar, M.; Nagy, S.; Schwarz, S.; Schweikhard, L.; Yazidjian, C. The Ramsey method in high-precision mass spectrometry with Penning traps: Experimental results. *Int. J. Mass Spectrom.* **2007**, *264*, 110–121. [CrossRef]
13. Kretzschmar, M. The Ramsey method in high-precision mass spectrometry with Penning traps: Theoretical foundations. *Int. J. Mass Spectrom.* **2007**, *264*, 122–145. [CrossRef]
14. Eliseev, S.; Blaum, K.; Block, M.; Droese, C.; Goncharov, M.; Minaya Ramirez, E.; Nesterenko, D.A.; Novikov, Y.N.; Schweikhard, L. Phase-Imaging Ion-Cyclotron-Resonance Measurements for Short-Lived Nuclides. *Phys. Rev. Lett.* **2013**, *110*, 082501. [CrossRef]
15. Eliseev, S.; Blaum, K.; Block, M.; Dörr, A.; Droese, C.; Eronen, T.; Goncharov, M.; Höcker, M.; Ketter, J.; Ramirez, E.M.; et al. A phase-imaging technique for cyclotron-frequency measurements. *Appl. Phys. B* **2014**, *114*, 107–128. [CrossRef]
16. Moore, F.L.; Brown, L.S.; Farnham, D.L.; Jeon, S.; Schwinberg, P.B.; Van Dyck, R.S. Cyclotron resonance with 10^{-11} resolution: Anharmonic detection and beating a coherent drive with the noise. *Phys. Rev. A* **1992**, *46*, 2653–2667. [CrossRef]
17. Cornell, E.A.; Weisskoff, R.M.; Boyce, K.R.; Flanagan, R.W.; Lafyatis, G.P.; Pritchard, D.E. Single-ion cyclotron resonance measurement of $M(CO^+)/M(N_2^+)$. *Phys. Rev. Lett.* **1989**, *63*, 1674–1677. [CrossRef]
18. Shi, W.; Redshaw, M.; Myers, E.G. Atomic masses of ^{32,33}S, ^{84,86}Kr, and ^{129,132}Xe with uncertainties $\leqslant$ 0.1 ppb. *Phys. Rev. A* **2005**, *72*, 022510. [CrossRef]
19. Heiße, F.; Rau, S.; Köhler-Langes, F.; Quint, W.; Werth, G.; Sturm, S.; Blaum, K. High-precision mass spectrometer for light ions. *Phys. Rev. A* **2019**, *100*, 022518. [CrossRef]
20. Blaum, K.; Bollen, G.; Herfurth, F.; Kellerbauer, A.; Kluge, H.J.; Kuckein, M.; Sauvan, E.; Scheidenberger, C.; Schweikhard, L. Carbon clusters for absolute mass measurements at ISOLTRAP. *Eur. Phys. J. A* **2002**, *15*, 245–248. [CrossRef]
21. Chaudhuri, A.; Block, M.; Eliseev, S.; Ferrer, R.; Herfurth, F.; Martín, A.; Marx, G.; Mukherjee, M.; Rauth, C.; Schweikhard, L.; et al. Carbon-cluster mass calibration at SHIPTRAP. *Eur. Phys. J. D* **2007**, *45*, 47–53. [CrossRef]
22. Elomaa, V.V.; Eronen, T.; Hager, U.; Jokinen, A.; Kessler, T.; Moore, I.D.; Rahaman, S.; Weber, C.; Äystö, J. Development of a carbon-cluster ion source for JYFLTRAP. *Nucl. Instrum. Methods Phys. Res. Sect. B Beam Interact. Mater. Atoms.* **2008**, *266*, 4425–4428. [CrossRef]
23. Scielzo, N.D.; Caldwell, S.; Savard, G.; Clark, J.A.; Deibel, C.M.; Fallis, J.; Gulick, S.; Lascar, D.; Levand, A.F.; Li, G.; et al. Double-β-decay Q values of ^{130}Te, ^{128}Te, and ^{120}Te. *Phys. Rev. C* **2009**, *80*, 025501. [CrossRef]
24. Smorra, C.; Blaum, K.; Eberhardt, K.; Eibach, M.; Ketelaer, J.; Ketter, J.; Knuth, K.; Nagy, S. A carbon-cluster laser ion source for TRIGA-TRAP. *J. Phys. B At. Mol. Opt. Phys.* **2009**, *42*, 154028. [CrossRef]
25. Izzo, C.; Bollen, G.; Bustabad, S.; Eibach, M.; Gulyuz, K.; Morrissey, D.J.; Redshaw, M.; Ringle, R.; Sandler, R.; Schwarz, S.; et al. A laser ablation source for offline ion production at LEBIT. *Nucl. Instrum. Methods Phys. Res. Sect. B Beam Interact. Mater. Atoms.* **2016**, *376*, 60–63. [CrossRef]
26. Eliseev, S.; Blaum, K.; Block, M.; Chenmarev, S.; Dorrer, H.; Düllmann, C.E.; Enss, C.; Filianin, P.E.; Gastaldo, L.; Goncharov, M.; et al. Direct Measurement of the Mass Difference of ^{163}Ho and ^{163}Dy Solves the Q-Value Puzzle for the Neutrino Mass Determination. *Phys. Rev. Lett.* **2015**, *115*, 062501. [CrossRef] [PubMed]
27. Schneider, F.; Beyer, T.; Blaum, K.; Block, M.; Chenmarev, S.; Dorrer, H.; Düllmann, C.E.; Eberhardt, K.; Eibach, M.; Eliseev, S.; et al. Preparatory studies for a high-precision Penning-trap measurement of the 163Ho electron capture Q-value. *Eur. Phys. J. A* **2015**, *51*, 89. [CrossRef]
28. Eibach, M.; Beyer, T.; Blaum, K.; Block, M.; Düllmann, C.E.; Eberhardt, K.; Grund, J.; Nagy, S.; Nitsche, H.; Nörtershäuser, W.; et al. Direct high-precision mass measurements on ^{241,243}Am, ^{244}Pu, and ^{249}Cf. *Phys. Rev. C* **2014**, *89*, 064318. [CrossRef]
29. Bhandari, R.; Horana Gamage, M.; Gamage, N.D.; Redshaw, M. Investigation of Ho ion production with a laser ablation ion source. *J. Phys. Conf. Ser.* **2022**, *2244*, 012076. [CrossRef]
30. Bhandari, R.; Bollen, G.; Brunner, T.; Gamage, N.D.; Hamaker, A.; Hockenbery, Z.; Gamage, M.H.; Keblbeck, D.K.; Leach, K.G.; Puentes, D.; et al. First direct ^{7}Be electron capture Q-value measurement towards high-precision BSM neutrino physics searches. *Phys. Rev. Lett.* **2023**, *to be submitted*. [CrossRef]
31. Gulyuz, K.; Ariche, J.; Bollen, G.; Bustabad, S.; Eibach, M.; Izzo, C.; Novario, S.J.; Redshaw, M.; Ringle, R.; Sandler, R.; et al. Determination of the direct double-β-decay Q value of ^{96}Zr and atomic masses of $^{90-92,94,96}$Zr and $^{92,94-98,100}$Mo. *Phys. Rev. C* **2015**, *91*, 055501. [CrossRef]
32. Eibach, M.; Bollen, G.; Gulyuz, K.; Izzo, C.; Redshaw, M.; Ringle, R.; Sandler, R.; Valverde, A.A. Double resonant enhancement in the neutrinoless double-electron capture of ^{190}Pt. *Phys. Rev. C* **2016**, *94*, 015502. [CrossRef]
33. Sandler, R.; Bollen, G.; Gamage, N.D.; Hamaker, A.; Izzo, C.; Puentes, D.; Redshaw, M.; Ringle, R.; Yandow, I. Investigation of the potential ultralow Q-value β-decay candidates ^{89}Sr and ^{139}Ba using Penning trap mass spectrometry. *Phys. Rev. C* **2019**, *100*, 024309. [CrossRef]
34. Gamage, N.D.; Bollen, G.; Eibach, M.; Gulyuz, K.; Izzo, C.; Kandegedara, R.M.E.B.; Redshaw, M.; Ringle, R.; Sandler, R.; Valverde, A.A. Precise determination of the ^{113}Cd fourth-forbidden non-unique β-decay Q value. *Phys. Rev. C* **2016**, *94*, 025505. [CrossRef]
35. Kandegedara, R.M.E.B.; Bollen, G.; Eibach, M.; Gamage, N.D.; Gulyuz, K.; Izzo, C.; Redshaw, M.; Ringle, R.; Sandler, R.; Valverde, A.A. β-decay Q values among the $A = 50$ Ti-V-Cr isobaric triplet and atomic masses of ^{46,47,49,50}Ti,^{50,51} V, and $^{50,52--54}$Cr. *Phys. Rev. C* **2017**, *96*, 044321. [CrossRef]

36. Sandler, R.; Bollen, G.; Dissanayake, J.; Eibach, M.; Gulyuz, K.; Hamaker, A.; Izzo, C.; Mougeot, X.; Puentes, D.; Quarati, F.G.A.; et al. Direct determination of the ^{138}La β-decay Q value using Penning trap mass spectrometry. *Phys. Rev. C* **2019**, *100*, 014308. [CrossRef]
37. Quarati, F.G.A.; Bollen, G.; Dorenbos, P.; Eibach, M.; Gulyuz, K.; Hamaker, A.; Izzo, C.; Keblbeck, D.K.; Mougeot, X.; Puentes, D.; et al. Measurements and computational analysis of the natural decay of ^{176}Lu. *Phys. Rev. C* **2023**, *107*, 024313. [CrossRef]
38. Amplitude-Laser: Surelite. Available online: https://amplitude-laser.com (accessed on 8 August 2023).
39. Redshaw, M.; Bryce, R.A.; Hawks, P.; Gamage, N.D.; Hunt, C.; Kandegedara, R.M.E.B.; Ratnayake, I.S.; Sharp, L. Status and outlook of CHIP-TRAP: The Central Michigan University high precision Penning trap. *Nucl. Instrum. Methods Phys. Res. Sect. B Beam Interact. Mater. Atoms.* **2016**, *376*, 302–306. [CrossRef]
40. Horana Gamage, M.; Arnold, A.L.; Bhandari, R.; Gamage, N.D.; Purcell, Z.; Sandler, R.; Redshaw, M. Design and characterization of Ion sources for CHIP-TRAP. *Hyperfine Interact.* **2019**, *240*, 93. [CrossRef]
41. HTW Hochtemperatur- Werkstoffe GmbH. Available online: http://www.htw-germany.com (accessed on 8 August 2023).
42. Horana Gamage, M.; Bhandari, R.; Gamage, N.D.; Keblbeck, D.; Redshaw, M. Design and simulations for a Penning Ion Trap Source for the CHIP-TRAP Mass Spectrometer. *J. Phys. Conf. Ser.* **2022**, *2244*, 012087. [CrossRef]
43. K&J Magnetics, Inc. Part #RXC88. Available online: https://www.kjmagnetics.com (accessed on 8 August 2023).
44. Gabrielse, G.; Mackintosh, F. Cylindrical Penning traps with orthogonalized anharmonicity compensation. *Int. J. Mass Spectrom. Ion Process.* **1984**, *57*, 1–17. [CrossRef]
45. Ted Pella, Inc. Part #1403. Available online: https://www.tedpella.com (accessed on 8 August 2023).
46. Gamage, M.H. High Precision Mass Measurement of ^{75}As to Identify Potential Ultra-low Q value Electron Capture Decay Branch in ^{75}Se and Commissioning of a Penning Ion Trap Source for CHIP-TRAP at CMU. Ph.D. Thesis, Central Michigan University, Mount Pleasant, MI, USA, 2023. Available online: https://scholar.google.com/scholar?cluster=3333153868775418497&hl=en&oi=scholarr (accessed on 8 August 2023).
47. Wolf, R.N.; Eritt, M.; Marx, G.; Schweikhard, L. A multi-reflection time-of-flight mass separator for isobaric purification of radioactive ion beams. *Hyperfine Interact.* **2011**, *199*, 115–122. [CrossRef]
48. Ito, Y.; Schury, P.; Wada, M.; Naimi, S.; Sonoda, T.; Mita, H.; Arai, F.; Takamine, A.; Okada, K.; Ozawa, A.; et al. Single-reference high-precision mass measurement with a multireflection time-of-flight mass spectrograph. *Phys. Rev. C* **2013**, *88*, 011306. [CrossRef]
49. Schultz, B.E.; Kelly, J.M.; Nicoloff, C.; Long, J.; Ryan, S.; Brodeur, M. Construction and simulation of a multi-reflection time-of-flight mass spectrometer at the University of Notre Dame. *Nucl. Instrum. Methods Phys. Res. Sect. B Beam Interact. Mater. Atoms.* **2016**, *376*, 251–255. [CrossRef]
50. Wolf, R.N.; Marx, G.; Rosenbusch, M.; Schweikhard, L. Static-mirror ion capture and time focusing for electrostatic ion-beam traps and multi-reflection time-of-flight mass analyzers by use of an in-trap potential lift. *Int. J. Mass Spectrom.* **2012**, *313*, 8–14. [CrossRef]
51. Bradbury, N.E.; Nielsen, R.A. Absolute Values of the Electron Mobility in Hydrogen. *Phys. Rev.* **1936**, *49*, 388–393. [CrossRef]
52. Comisarow, M.B.; Marshall, A.G. Theory of Fourier transform ion cyclotron resonance mass spectroscopy. I. Fundamental equations and low-pressure line shape. *J. Chem. Phys.* **1975**, *64*, 110. [CrossRef]
53. Comisarow, M.B.; Marshall, A.G. Signal modeling for ion cyclotron resonance. *J. Chem. Phys.* **1978**, *69*, 4097. [CrossRef]
54. Marshall, A.G.; Comisarow, M.B.; Parisod, G. Relaxation and spectral line shape in Fourier transform ion resonance spectroscopya. *J. Chem. Phys.* **1979**, *71*, 4434. [CrossRef]
55. Stahl-Electronics. Available online: https://www.stahl-electronics.com (accessed on 8 August 2023).
56. Marshall, A.G.; Wang, T.C.L.; Ricca, T.L. Tailored excitation for Fourier transform ion cyclotron mass spectrometry. *J. Am. Chem. Soc.* **1985**, *107*, 7893–7897. [CrossRef]
57. Guan, S.; Marshall, A.G. Stored waveform inverse Fourier transform (SWIFT) ion excitation in trapped-ion mass spectometry: Theory and applications. *Int. J. Mass Spectrom. Ion Process.* **1996**, *157-158*, 5–37. [CrossRef]
58. Kwiatkowski, A.A.; Bollen, G.; Redshaw, M.; Ringle, R.; Schwarz, S. Isobaric beam purification for high precision Penning trap mass spectrometry of radioactive isotope beams with SWIFT. *Int. J. Mass Spectrom.* **2015**, *379*, 9–15. [CrossRef]
59. Hamaker, A.; Bollen, G.; Eibach, M.; Izzo, C.; Puentes, D.; Redshaw, M.; Ringle, R.; Sandler, R.; Schwarz, S.; Yandow, I. SIPT—An ultrasensitive mass spectrometer for rare isotopes. *Hyperfine Interact.* **2019**, *240*, 34. [CrossRef]
60. Ringle, R.; Schwarz, S.; Bollen, G. Penning trap mass spectrometry of rare isotopes produced via projectile fragmentation at the LEBIT facility. *Int. J. Mass Spectrom.* **2013**, *349-350*, 87–93. [CrossRef]
61. Cornell, E.A.; Weisskoff, R.M.; Boyce, K.R.; Pritchard, D.E. Mode coupling in a Penning trap: π pulses and a classical avoided crossing. *Phys. Rev. A* **1990**, *41*, 312–315. [CrossRef]
62. Rainville, S. A Two-Ion Balance for High Precision Mass Spectrometry. Ph.D. Thesis, Massachusetts Institute of Technology, Cambridge, MA, USA, 2003. Available online: https://dspace.mit.edu/handle/1721.1/16934 (accessed on 8 August 2023).
63. Thompson, J.K.; Rainville, S.; Pritchard, D.E. Cyclotron frequency shifts arising from polarization forces. *Nature* **2004**, *430*, 58–61. [CrossRef]
64. Rainville, S.; Thompson, J.K.; Myers, E.G.; Brown, J.M.; Dewey, M.S.; Kessler, E.G.; Deslattes, R.D.; Börner, H.G.; Jentschel, M.; Mutti, P.; et al. A direct test of E = mc2. *Nature* **2005**, *438*, 1096–1097. [CrossRef]

65. Lincoln, D.L.; Baker, R.; Benjamin, A.L.; Bollen, G.; Redshaw, M.; Ringle, R.; Schwarz, S.; Sonea, A.; Valverde, A.A. Development of a high-precision Penning trap magnetometer for the LEBIT facility. *Int. J. Mass Spectrom.* **2015**, *379*, 1–8. [CrossRef]
66. Redshaw, M.; Benjamin, A.L.; Bollen, G.; Ferrer, R.; Lincoln, D.L.; Ringle, R.; Schwarz, S.; Valverde, A.A. Fabrication and characterization of field emission points for ion production in Penning trap applications. *Int. J. Mass Spectrom.* **2015**, *379*, 187–193. [CrossRef]
67. Kimball Physics: LaB_6. Available online: https://www.kimballphysics.com/product-category/cathodes-emitters/ (accessed on 8 August 2023).
68. NF Corp: SA-421F5 Amplfier. Available online: https://www.nfcorp.co.jp/english/pro/mi/loc/pre/sa/index.html (accessed on 8 August 2023).
69. Schweihard, L.; Lindinger, M.; Kluge, H.J. Quadrupole-detection FT-ICR mass spectrometry. *Int. J. Mass Spectrom. Ion Process.* **1990**, *98*, 25–33. [CrossRef]
70. Gamage, N.D. Design and Commissioning of the CHIP-TRAP Mass Spectrometer at CMU. Ph.D. Thesis, Central Michigan University, Mount Pleasant, MI, USA, 2021. Available online: https://scholarly.cmich.edu/ (accessed on 8 August 2023).